TR
Technical Report

Technical Report - WP4 - Version 1.0

Modulation and Detection for High Doppler Channels: An Overview on OTFS Modulation

Thi My Chinh Chu and
Hans-Jürgen Zepernick

BTH, June, 2023

BTH
Department of Computer Science, 2023

Blekinge Institute of Technology
Valhallavägen 1
SE-37179 Karlskrona
Sweden

Revision History

Revision	Date	Comments
0.1	14/12/20	Draft version
1.0	30/06/23	Initial release

Acknowledgments

This work has been funded in part by the Swedish Governmental Agency for Innovation Systems under Grant 2019-02769, Project: Directed Air Data Link.

Contents

CHAPTER 1

Introduction

Technical specifications of the waveform design for the directed air data link regarding physical layer parameters have been discussed and used for performance simulation of modulation schemes for high Doppler channels. BTH and Saab have discussed suitable propagation environments and Doppler profiles that can be used for performance simulation. An orthogonal time frequency space (OTFS) modulation technique has been identified from a survey on modulation techniques for high Doppler channels. On this basis, a simulation framework has been established and a simulation campaign has been conducted to assess the bit error rate of such systems. The impact of velocity, carrier frequency, and multipath propagation on the bit error rate (BER) of OTFS and multiple-input multiple-output (MIMO) OTFS (MIMO-OTFS) modulation for the considered target application has been revealed. A 2×2 MIMO-OTFS system has been shown to provide the best performance among the considered scenarios offering high link reliability at relatively low signal-to-noise ratios.

1.1 Motivation

The development of 5G air interfaces along with the associated waveforms has sparked research on modulation and detection techniques for high Doppler channels in recent years. These efforts on novel physical layer techniques of mobile communication systems are needed to support diverse requirements and use cases. For example, scenarios such as vehicle-to-vehicle and vehicle-to-infrastructure systems require 5G air interfaces to cope with terminal speeds of up to 300 km/h while terminal speeds of 500 km/h are to be considered for high-speed train applications. As such, promising approaches from the research on 5G air interfaces for modulation and detection in high Doppler channels may be translated to the particulars of objects traveling with supersonic speeds, i.e., exceeding the speed of sound.

In particular, OTFS modulation has been proposed to cope with high Doppler channels, large antenna arrays such as massive MIMO systems, and high carrier frequencies such as millimeter waves [1]–[3]. OTFS can be seen as a generalization of code division multiples access (CDMA) and orthogonal frequency division multiplexing (OFDM), thus, inheriting some of the benefits of these two schemes. Given that CDMA has been dominating 3G mobile systems while various OFDM based techniques have been developed for 4G and 5G mobile systems, in the sequel, we will provide some background on OFDM as predecessor air interface of contemporary mobile systems with respect to OTFS modulation.

OFDM is a multicarrier modulation technique that has been developed to cope with frequency selective channels in which different frequencies of a signal experience uncorrelated fading. A solution to this problem is to break a wideband channel into multiple parallel narrowband channels by means of orthogonal channels. In other words, high data rate transmission over frequency selective fading channels is broken down into a set of parallel low data rate transmissions over flat fading channels. Mathematically, the fundamental operation of an OFDM transmitter can be expressed as inverse discrete Fourier transform (IDFT)

$$s[n] = \mathrm{IDFT}\{X[i]\} = \frac{1}{\sqrt{N}} \sum_{i=0}^{N-1} X[i] e^{j\frac{2\pi ni}{N}}, \quad 0 \leq n \leq N-1 \tag{1.1}$$

and the OFDM receiver performs a discrete Fourier transform (DFT)

$$X[i] = \mathrm{DFT}\{s[n]\} = \frac{1}{\sqrt{N}} \sum_{n=0}^{N-1} s[n] e^{-j\frac{2\pi ni}{N}}, \quad 0 \leq i \leq N-1 \tag{1.2}$$

where i and n denote the subcarrier index and discrete time index, respectively, and $X[i]$, $0 \leq i \leq N-1$ characterizes the frequency content of the discrete time sequence $s[n]$, $0 \leq n \leq N-1$.

At the transmitter, OFDM performs a serial-to-parallel conversion to decompose the wide transmission bandwidth into a number of narrow contiguous subbands or carriers. Each carrier is individually modulated, e.g., quadrature amplitude modulation (QAM) resulting in a complex stream of N parallel QAM symbols $X[0]$, $X[1]$, ..., $X[N-1]$. This complex symbol stream represents the discrete frequency components of the OFDM modulator output $s(t)$. The corresponding inverse operations are performed at the OFDM receiver. The DFT at the receiver and IDFT at the transmitter can be efficiently implemented using the fast Fourier transform (FFT) and inverse FFT (IFFT). The benefits of OFDM modulation include the following:

- Bandwidth efficient.
- Easy to implement at the transmitter and receiver with IFFT and FFT.
- Simple detection with a one tap equalizer.
- Robust against frequency selective fading due to using narrow orthogonal subcarriers.
- Eliminates adjacent subcarrier crosstalk.

On the other hand, drawbacks of OFDM modulation can be summarized as follows:

- Expensive linear amplifiers are needed because the amplitude of the transmit signal can change significantly.
- Multiple and high Doppler shifts are difficult to equalize.
- Because the subchannel gains are not equal, the worst subchannel determines the performance.

1.2 Structure of the Technical Report

This technical report is organized as follows. Chapter 2 presents fundamentals of wireless channel representations in terms of the four Bello functions, i.e., time-variant channel impulse response, time-frequency channel, delay-Doppler channel, and Doppler-variant transfer function. Chapter 3 provides concepts of OTFS modulation including mathematical descriptions of the transmitter and receiver functions, and OTFS modulation for ideal pulses. Chapter 4 translates the various transforms of the input-output relation of the OTFS transmitter and receiver system into matrix form. Chapter 5 gives a mathematical formulation of MIMO-OTFS modulation using the matrix form approach. Chapter 6 presents numerical results of the performance of OTFS and MIMO-OTFS modulation in terms of BER with simulation parameters being selected in view of specification of the directed air data link. Chapter 7 points out the wide range of applications of OTFS modulation stretching from OTFS channel estimation to path division multiple access for massive MIMO-OTFS.

CHAPTER 2

Wireless Channel Representations

A wireless channel may be envisaged as an element which transforms input signals into output signals. The impulse response is a wideband channel characterisation and contains all information necessary to simulate or analyse any type of radio transmission through the channel. A wireless channel may be modeled as a linear filter with a time varying impulse response $h(t,\tau)$ where t represents the time variation due to motion and τ represents the channel multipath delay for a fixed value of t. Let $s(t)$ denote the transmitted signal, then the received signal $r(t)$ is given by

$$r(t) = \int_{-\infty}^{\infty} s(t-\tau)h(t,\tau)d\tau \tag{2.1}$$

or in more compact form by using the linear convolution operator $*$ as

$$r(t) = s(t) * h(t,\tau) \tag{2.2}$$

2.1 Bello Functions

In view of (2.1) and (2.2), a radio channel may be considered as a linear filter. Because a radio channel is generally time-variant, the transmission characteristics of an equivalent filter must also be time-varying. The inputs and outputs of a linear filter can be described in the time domain and the frequency domain. For a time-variant filter having two variables t and τ, four possible system functions are obtained which in the context of radio channels are know as Bello functions [4]:

- **Input delay-spread function (Linear time-variant channel)**

  A popular model of a time-variant channel with specular scattering is the channel's time-variant impulse response or input delay-spread function $h(t,\tau)$. The received signal in a multipath channel consists of a series of attenuated, time-delayed, phase shifted replicas of the transmitted signal. As such, the time varying discrete-time baseband impulse response model for a multipath channel can be formulated as

$$h(t,\tau) = \sum_{i=0}^{N-1} a_i(t,\tau)\exp\left[j2\pi f_c\tau_i(t) + \phi(t,\tau)\right]\delta(t-\tau_i(t)) \tag{2.3}$$

where N denotes the number of paths, $a_i(t,\tau)$ denotes the attenuation of the ith path, $\tau_i(t)$ is the time delay induced by the ith path, $\phi(t,\tau)$ represent a phase shift, f_c denotes the carrier frequency, and $\delta(\cdot)$ is the Dirac impulse.

- **Time-variant transfer function (Time-frequency channel)**

  Another approach is to express the output time function in terms of the input spectrum to the channel equivalent filter. This function is known as the time-variant transfer function $H(t,f)$ and is the Fourier transform of the input delay-spread function $h(t,\tau)$ with respect to the delay variable τ:

$$H(t,f) = \int_{-\infty}^{\infty} h(t,\tau)\exp(-j2\pi f\tau)d\tau \tag{2.4}$$

  The time-variant transfer function $H(t,f)$ represents the frequency transfer function of the channel as a function of time.

- **Doppler-variant transfer function (Doppler-frequency channel)**

  The time-variant transfer function $H(t,f)$ can be transformed with respect to the time variable t which results in the Doppler-variant transfer function

$$B(\nu,f) = \int_{-\infty}^{\infty} H(t,f)\exp(-j2\pi\nu t)dt \tag{2.5}$$

  In this representation, the frequency-shift variable ν can be visualized as the Doppler shift experienced in the channel.

- **Delay-Doppler spread function (Delay-Doppler channel)**

  From the engineer's point of view, it would be useful to have a system function that simultaneously provides a description in both time-delay and Doppler spread domains. A characterisation which has the time-delay operation at the input and the Doppler-shift operation at the output can be termed a delay-Doppler channel

$$S(\nu,\tau) = \int_{-\infty}^{\infty} h(t,\tau)\exp(-j2\pi\nu t)dt \tag{2.6}$$

Figure 2.1 shows the relationship between the Bello functions that are given by Fourier transform $\mathcal{F}$, inverse Fourier transform $\mathcal{F}^{-1}$, symplectic finite Fourier transform SFFT, and inverse symplectic finite Fourier transform SFFT^{-1}. In the context of modulation in high Doppler channels, the relationship between the time-frequency channel $H(t,f)$ and the delay-Doppler channel $S(\nu,\tau)$ is of particular interest. While $H(t,f)$ is used to develop transceivers in the time-frequency plane to deal with delay spread (frequency-selective fading), $S(\nu,\tau)$ can be used to develop transceivers in the delay-Doppler plane to deal with high Doppler spread.

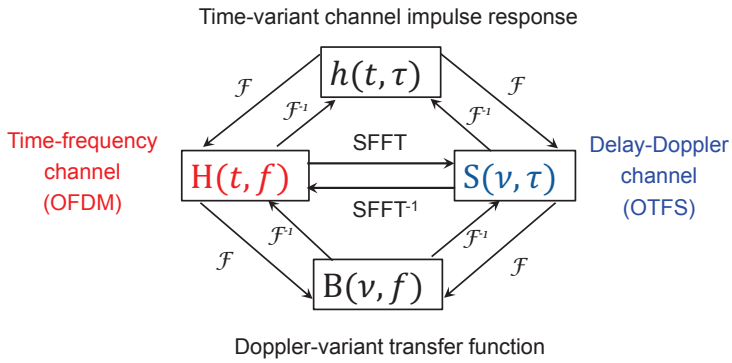

Figure 2.1: Relationships between the four Bello functions.

In preparation of the discussion about OTFS modulation, the received signal $r(t)$ in a linear time-variant channel may be expressed as

$$\begin{aligned} r(t) &= \int_{\infty}^{\infty} h(t,\tau)s(t-\tau)d\tau && \text{(Linear time-variant channel)} \\ &= \int_{\infty}^{\infty}\int_{\infty}^{\infty} S(\nu,\tau)s(t-\tau)e^{j\pi\nu t}d\tau d\nu && \text{(Delay-Doppler channel)} \\ &= \int_{\infty}^{\infty}\int_{\infty}^{\infty} H(t,f)S(f)e^{j\pi f t}df && \text{(Time-frequency channel)} \end{aligned} \tag{2.7}$$

The relationships between the delay-Doppler channel $S(\nu,\tau)$ (related to OTFS) and the time-frequency channel $H(t,f)$ (related to OFDM) are given by

$$S(\nu,\tau) = \int_{\infty}^{\infty}\int_{\infty}^{\infty} H(t,f)e^{-j2\pi(\nu t - f\tau)}dtdf \tag{2.8}$$

$$H(t,f) = \int_{\infty}^{\infty}\int_{\infty}^{\infty} S(\nu,\tau)e^{j2\pi(\nu t - f\tau)}d\tau d\nu \tag{2.9}$$

where time-frequency channel $H(t,f)$ and delay-Doppler channel $S(\nu,\tau)$ constitute a pair of symplectic Fourier transforms

$$H(t,f) \rightleftarrows S(\nu,\tau) \tag{2.10}$$

Symplectic Fourier transforms are double Fourier transforms with a symplectic ("symplektikos" being a Greek translation of Latin "complexus") inner product in the exponent, which in the considered context of OTFS modulation and demodulation is captured in (2.8) and (2.9) as

$$e^{-j2\pi(\nu t - f\tau)} = e^{-j2\pi\nu t}\cdot e^{+j2\pi f\tau} \tag{2.11}$$

$$e^{j2\pi(\nu t - f\tau)} = e^{+j2\pi\nu t}\cdot e^{-j2\pi f\tau} \tag{2.12}$$

As such, inheriting the foundations of Fourier transforms, the discrete symplectic finite Fourier transform (SFFT) and inverse SFFT (ISFFT) of the periodized version $X_p[m,n]$ of $X[m,n]$ with period (M,N) are defined as

$$\begin{aligned} x_p[k,l] &= \mathrm{SFFT}(X_p[m,n]) \\ &= \frac{1}{\sqrt{MN}} \sum_{m=0}^{M-1} \sum_{n=0}^{N-1} X_p[m,n] e^{-j2\pi\left(\frac{mk}{M} - \frac{nl}{N}\right)} \end{aligned} \tag{2.13}$$

$$\begin{aligned} X_p[m,n] &= \mathrm{ISFFT}(x_p[k,l]) \\ &= \frac{1}{\sqrt{MN}} \sum_{k=0}^{M-1} \sum_{l=0}^{N-1} x_p[k,l] e^{j2\pi\left(\frac{ml}{M} - \frac{nk}{N}\right)} \end{aligned} \tag{2.14}$$

2.2 Time-Frequency and Delay-Doppler Grids

Figure 2.2 illustrates the mapping of the of sampled versions of the time-frequency channel $H(t,f)$ and delay-Doppler channel $S(\tau,\nu)$ to the time-frequency grid and the delay-Doppler grid using the following parameters:

- **Sampling of the time and frequency axes at intervals T and Δf**

$$\Delta f = \frac{B}{M} \tag{2.15}$$

$$T = \frac{1}{\Delta f} \tag{2.16}$$

  where $B = M\Delta f$ denotes the total bandwidth of the system and NT is the total duration of a packet comprising of N symbols of duration T.

- **Sampling of the delay and Doppler axes at intervals $\Delta\tau$ and $\Delta\nu$**

$$\Delta\tau = \frac{1}{M\Delta f} \tag{2.17}$$

$$\Delta\nu = \frac{1}{NT} = \frac{\Delta f}{N} \tag{2.18}$$

  where $\Delta\tau$ denotes the delay resolution and $\Delta\nu$ is the Doppler resolution.

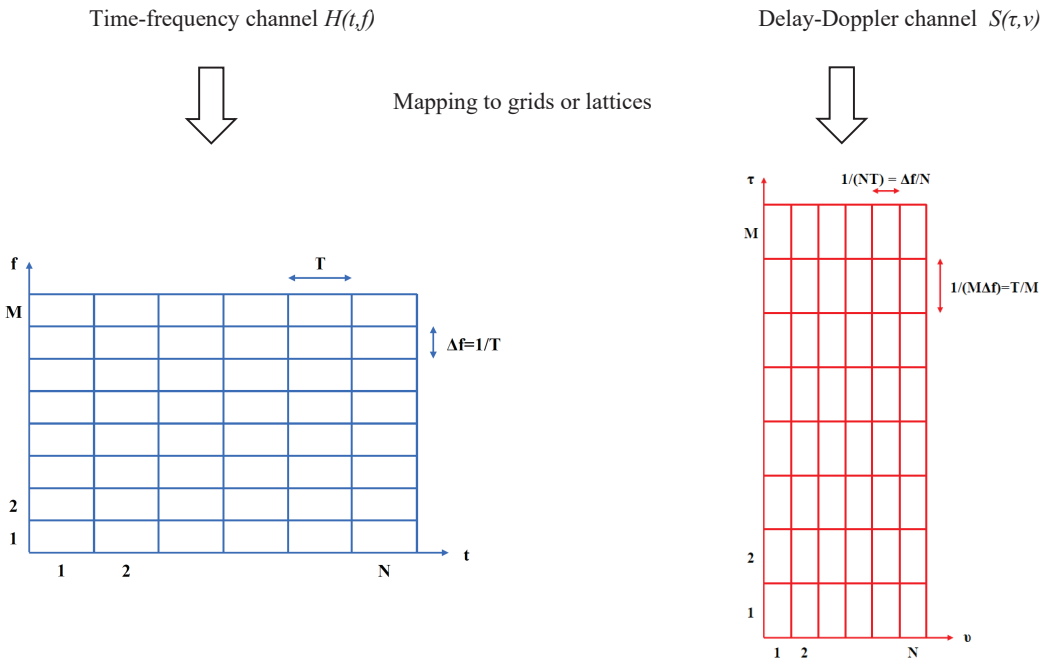

(a) Time-frequency grid

(b) Delay-Doppler grid

Figure 2.2: Considered wireless channel representations and their mappings to the time-frequency grid and the delay-Doppler grid.

CHAPTER 3

Orthogonal Time Frequency Space Modulation

Orthogonal time frequency space modulation was introduced as a two-dimensional modulation technique in the delay-Doppler domain. In this chapter, fundamentals and notations of OTFS modulation are provided to the extent needed for the understanding of its application in directed air data links. The reader is referred to, e.g., [1], [2], [5]–[8], for a comprehensive coverage of OTFS modulation.

A block diagram of OTFS modulation illustrating the main functions at the transmitter and receiver is shown in Figure 3.1. At the transmitter, an OTFS modulator first performs an ISFFT of the information symbols $x[n, m]$ in the delay-Doppler domain to symbols $X[n, m]$ in the time-frequency domain. Then, the symbols $X[n, m]$ are transformed into a time domain signal $s(t)$ using the Heisenberg transform. At the receiver, an OTFS demodulator first maps the received time domain signal $r(t)$ to a symbol $Y[t, f]$ in the time-frequency domain using the Wigner transform. Then, the symbol $Y[t, f]$ is converted into a received information symbol $y[n, m]$ in the delay-Doppler domain using the SFFT.

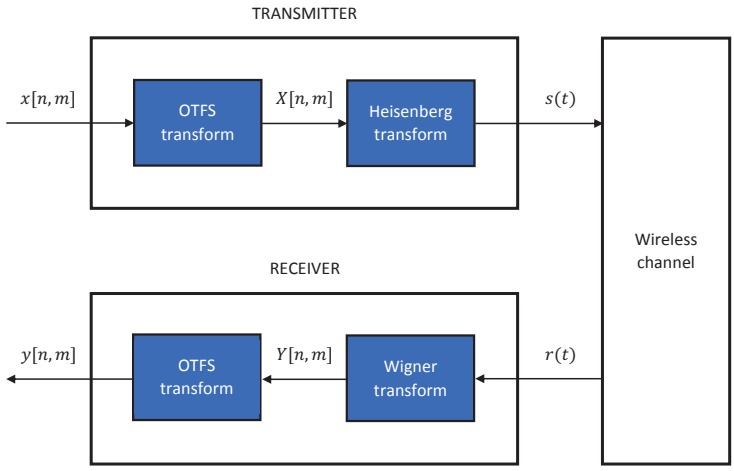

Figure 3.1: Block diagram of an OTFS modulator.

The following sections provide a mathematical description of the components at the OTFS transmitter and receiver, and the OTFS modulation for ideal pulses as a preparation of the matrix description of the input-output relation of an OTFS system.

3.1 OTFS Modulation - Transmitter

Mathematically, an OTFS modulator applies the ISFFT defined in (2.14) to the information symbols $x[k,l]$ into the delay-Doppler domain of symbols $X[n,m]$ in the time-frequency domain as

$$X[n,m] = \frac{1}{\sqrt{NM}} \sum_{k=0}^{N-1} \sum_{l=0}^{M-1} x[k,l] e^{j2\pi\left(\frac{nk}{N} - \frac{ml}{M}\right)} \tag{3.1}$$

The mapping of the discrete symbols of the delay-Dopper domain $X[n,m]$ into a continuous-time transmit signal $s(t)$, also referred to as waveform, includes pulse shaping with a transmit pulse $g_{tx}(t)$ and an associated receive pulse $g_{rx}(t)$. To support matched filtering at the receiver and eliminate cross-symbol interference at the OTFS demodulator, bi-orthogonal pulses with respect to translations in time T and frequency Δf are used, i.e.,

$$\int g_{tx}(t) g_{rx}^{*}(t - nT) e^{j2\pi m\Delta f(t-nT)} dt = \delta(m)\delta(n) \tag{3.2}$$

Given a suitable transmit pulse $g_{tx}(t)$, the transmit signal $s(t)$ is obtained by performing the Heisenberg transform as follows:

$$s(t) = \sum_{m=0}^{M-1} \sum_{n=0}^{N-1} X[n,m] g_{tx}(t - nT) e^{j2\pi m\Delta f(t-nT)} \tag{3.3}$$

Note that the transform in (3.3) simplifies to an inverse discrete Fourier transform (IDFT) for $N = 1$ and a rectangular pulse $g_{tx}(t) = \text{rect}\left(\frac{t}{T}\right)$:

$$s(t) = \sum_{m=0}^{M-1} X[m] e^{j2\pi m\Delta f t} \tag{3.4}$$

As the IDFT in (3.4) basically represents the modulation of symbols to different frequency sub-bands as in OFDM, the Heisenberg transform in (3.3) may be considered as a generalization of OFDM.

3.2 OTFS Modulation - Receiver

Regarding OTFS demodulation, the received signal $r(t)$ of an OTFS modulation system can be obtained as [3]

$$r(t) = \int H(t,f) S(f) e^{j2\pi f t} df \tag{3.5}$$

where $H(t,f)$ is the time-frequency channel and $S(f) = \mathcal{F}(s(t))$ is the frequency spectrum of the continuous-time transmit signal $s(t)$.

Similar as the Heisenberg transform converts a symbol $X[n,m]$ into a signal $s(t)$, the Wigner transform converts a signal $r(t)$ into a symbol $Y[n,m]$ as follows. First, a matched filter $g_{rx}^*(t)$ with respect to the transmit pulse $g_{tx}(t)$ is used to calculate the cross-ambiguity function [3]

$$Y(t,f) = \int g_{rx}^*(t'-t) r(t') e^{-j2\pi f(t'-t)} dt' \tag{3.6}$$

Then, the cross-ambiguity function $Y(t,f)$ of the received signal in the time-frequency domain is sampled in time $t = nT$ and frequency $f = m\Delta f$. This sampling results in the symbols $Y[n,m]$ in the time-frequency domain as the matched filter output, i.e.,

$$Y[n,m] = Y(t,f)|_{t=nT, f=m\Delta f} \tag{3.7}$$

After the Wigner transform, the obtained symbols $Y[n,m]$ are transformed into the delay-Doppler domain using the ISFFT, i.e.,

$$y[k,l] = \frac{1}{\sqrt{NM}} \sum_{n=0}^{N-1} \sum_{m=0}^{M-1} Y[n,m] e^{-j2\pi\left(\frac{nk}{N} - \frac{ml}{M}\right)} \tag{3.8}$$

3.3 OTFS Modulation for Ideal Pulses

Let the bi-orthogonal condition stated in (3.2) hold for the pulses $g_{tx}^*(t)$ (transmit pulse) and $g_{rx}(t)$ (matched filter) which implies that these ideal pulses can be perfectly localized in time and frequency. Further, let the delay-Doppler channel $S(\tau,\nu)$ have finite support in both variables τ and ν, i.e.,

$$S(\tau,\nu) = \begin{cases} f(\tau,\nu) & \text{for } |\tau| \leq \tau_{max}, \quad |\nu| \leq \nu_{max} \\ 0 & \text{otherwise} \end{cases} \tag{3.9}$$

In addition, assume that the cross-ambiguity function $A_{g_{tx},g_{rx}}(\tau,\nu)$ also has finite support, such that the following holds for $n \neq 0$ and $m \neq 0$ [1]:

$$A_{g_{tx},g_{rx}}(\tau,\nu) = 0 \text{ for } \tau \in (nT - \tau_{max}, nT + \tau_{max}), \quad \nu \in (m\Delta f - \nu_{max}, m\Delta f + \nu_{max}) \tag{3.10}$$

Then, the input-output relation in the time-frequency domain can be written as

$$Y[n,m] = H[n,m] X[n,m] \tag{3.11}$$

where [3]

$$H[n,m] = \int\int S(\tau,\nu) e^{j2\pi\nu nT} e^{-j2\pi m\Delta f \tau} d\tau d\nu \tag{3.12}$$

In preparation of a matrix representation of OTFS modulation, the components of the signaling in the delay-Doppler domain can be obtained from (3.11) using the discrete delay-Doppler channel $S(k,l)$ as [3]

$$H[n,m] = \sum_{k=0}^{N-1}\sum_{l=0}^{M-1} S[k,l]e^{j2\pi\left(\frac{nk}{N}-\frac{ml}{M}\right)} \tag{3.13}$$

Substituting (3.13) in (3.11) and then substituting (3.1) into the obtained result gives

$$\begin{aligned} Y[n,m] &= \left[\sum_{k=0}^{N-1}\sum_{l=0}^{M-1} S[k,l]e^{j2\pi\left(\frac{nk}{N}-\frac{ml}{M}\right)}\right] X[n,m] \\ &= \left[\sum_{k=0}^{N-1}\sum_{l=0}^{M-1} S[k,l]e^{j2\pi\left(\frac{nk}{N}-\frac{ml}{M}\right)}\right]\left[\frac{1}{\sqrt{NM}}\sum_{k=0}^{N-1}\sum_{l=0}^{M-1} x[k,l]e^{j2\pi\left(\frac{nk}{N}-\frac{ml}{M}\right)}\right] \\ &= \frac{1}{\sqrt{NM}}\left[\sum_{k=0}^{N-1}\sum_{l=0}^{M-1} S[k,l]e^{j2\pi\left(\frac{nk}{N}-\frac{ml}{M}\right)}\right]\left[\sum_{k=0}^{N-1}\sum_{l=0}^{M-1} x[k,l]e^{j2\pi\left(\frac{nk}{N}-\frac{ml}{M}\right)}\right] \end{aligned} \tag{3.14}$$

Finally, the SFFT is used to covert the symbols $Y[n,m]$ of the time-frequency domain into symbols $y[k,l]$ of the delay-Doppler domain:

$$\begin{aligned} y[k,l] &= \frac{1}{\sqrt{NM}}\sum_{n=0}^{N-1}\sum_{m=0}^{M-1} Y[n,m]e^{-j2\pi\left(\frac{nk}{N}-\frac{ml}{M}\right)} \\ &= \frac{1}{NM}\sum_{n=0}^{N-1}\sum_{m=0}^{M-1} \\ &\times\left\{\left[\sum_{k=0}^{N-1}\sum_{l=0}^{M-1} S[k,l]e^{j2\pi\left(\frac{nk}{N}-\frac{ml}{M}\right)}\right]\left[\sum_{k=0}^{N-1}\sum_{l=0}^{M-1} x[k,l]e^{j2\pi\left(\frac{nk}{N}-\frac{ml}{M}\right)}\right]\right\} \\ &\times e^{-j2\pi\left(\frac{nk}{N}-\frac{ml}{M}\right)} \end{aligned} \tag{3.15}$$

CHAPTER 4

OTFS Input-Output Relation in Matrix Form

The expressions describing the relationships between the different channel domains given in (3.13), (3.14), and (3.15), use the following transform:

$$\begin{aligned} a^{DD}[k,l] &= \frac{1}{NM}\sum_{n=0}^{N-1}\sum_{m=0}^{M-1} A^{TF}[n,m]e^{j2\pi\left(\frac{nk}{N}-\frac{ml}{M}\right)} \\ &= \frac{1}{NM}\sum_{n=0}^{N-1} e^{j2\pi\frac{nk}{N}}\sum_{m=0}^{M-1} A^{TF}[n,m]e^{-j2\pi\frac{ml}{M}} \\ &= \frac{1}{NM}\sum_{n=0}^{N-1} e^{j2\pi\frac{nk}{N}}\mathbf{a}^{TF}[n]\cdot\mathbf{f}^{H}[l] \\ &= \frac{1}{NM}\mathbf{f}[k]\cdot\mathbf{A}^{TF}\cdot\mathbf{f}^{H}[l] \end{aligned} \tag{4.1}$$

where $A^{TF}[n,m]$ is a symbol in the time-frequency domain, $a^{DD}[k,l]$ is a symbol in the delay-Doppler domain, and $(\cdot)^H$ is the Hermitian operator (conjugate transpose). The transform between domains can then be expressed in matrix form as

$$\mathbf{A}^{DD} = \mathbf{F}\cdot\mathbf{A}^{TF}\cdot\mathbf{F}^{H} \tag{4.2}$$

where

$$\begin{aligned} \mathbf{A}^{DD} &= \left[a^{DD}[k,l]\right]_{M\times N} \\ &= \begin{bmatrix} a^{DD}[0,0] & a^{DD}[0,1] & \cdots & a^{DD}[0,N-1] \\ a^{DD}[1,0] & a^{DD}[1,1] & \cdots & a^{DD}[1,N-1] \\ \vdots & \vdots & \ddots & \vdots \\ a^{DD}[M-1,0] & a^{DD}[M-1,1] & \cdots & a^{DD}[M-1,N-1] \end{bmatrix} \end{aligned} \tag{4.3}$$

$$\begin{aligned}\mathbf{A}^{TF} &= \left[a^{TF}[n,m]\right]_{N\times M} \\ &= \begin{bmatrix} a^{TF}[0,0] & a^{TF}[0,1] & \cdots & a^{TF}[0,M-1] \\ a^{TF}[1,0] & a^{TF}[1,1] & \cdots & a^{TF}[1,M-1] \\ \vdots & \vdots & \ddots & \vdots \\ a^{TF}[N-1,0] & a^{TF}[N-1,1] & \cdots & a^{TF}[N-1,M-1] \end{bmatrix}\end{aligned} \tag{4.4}$$

The matrices $\mathbf{F}$ and $\mathbf{F}^H$ represent the SFFT and ISFFT, respectively, can be used to perform the Heisenberg and Wigner transform, and are given as

$$\begin{aligned}\mathbf{F} &= \frac{1}{\sqrt{NM}}\left[f[k,n]\right]_{N\times M} \\ &= \frac{1}{\sqrt{NM}}\begin{bmatrix} f[0,0] & f[0,1] & \cdots & f[0,M-1] \\ f[1,0] & f[1,1] & \cdots & f[1,M-1] \\ \vdots & \vdots & \ddots & \vdots \\ f[N-1,0] & f[N-1,1] & \cdots & f[N-1,M-1] \end{bmatrix} \\ &= \frac{1}{\sqrt{NM}}\begin{bmatrix} 1 & 1 & \cdots & 1 \\ 1 & e^{j2\pi\frac{1}{N}} & \cdots & e^{j2\pi\frac{M-1}{N}} \\ \vdots & \vdots & \ddots & \vdots \\ 1 & e^{j2\pi\frac{N-1}{N}} & \cdots & e^{j2\pi\frac{(N-1)(M-1)}{N}} \end{bmatrix}\end{aligned} \tag{4.5}$$

and

$$\begin{aligned}\mathbf{F}^H &= \frac{1}{\sqrt{NM}}\left[f^H[k,n]\right]_{N\times M} \\ &= \frac{1}{\sqrt{NM}}\begin{bmatrix} f^H[0,0] & f^H[0,1] & \cdots & f^H[0,M-1] \\ f^H[1,0] & f^H[1,1] & \cdots & f^H[1,M-1] \\ \vdots & \vdots & \ddots & \vdots \\ f^H[N-1,0] & f^H[N-1,1] & \cdots & f^H[N-1,M-1] \end{bmatrix} \\ &= \frac{1}{\sqrt{NM}}\begin{bmatrix} 1 & 1 & \cdots & 1 \\ 1 & e^{-j2\pi\frac{1}{N}} & \cdots & e^{-j2\pi\frac{M-1}{N}} \\ \vdots & \vdots & \ddots & \vdots \\ 1 & e^{-j2\pi\frac{N-1}{N}} & \cdots & e^{-j2\pi\frac{(N-1)(M-1)}{N}} \end{bmatrix}\end{aligned} \tag{4.6}$$

The general matrix formulation of the transforms between various domains can be used to write the transmitter and receiver functions, and eventually the OTFS

input-output relation, in compact matrix form. Furthermore, the matrix formulation allows to straightforwardly describe additional processing steps such as windowing or formulate extensions of OTFS modulation to MIMO-OTFS modulation.

4.1 OTFS Transmitter in Matrix Form

The OTFS transmit signal in the time-frequency domain is obtained from the OTFS symbols in the delay-Doppler domain by first performing an ISFFT, then applying the Heisenberg transfrom to obtain continuous-time signals, and finally a pulse shaping such that matched filtering can be used at the receiver. As such, the matrix representation of an OTFS transmitter can be formulated using (4.3)-(4.6) as

$$\mathbf{S} = \mathbf{G}_{tx}\mathbf{F}_M^H \left(\mathbf{F}_M \mathbf{X} \mathbf{F}_N^H\right) = \mathbf{G}_{tx}\mathbf{X}\mathbf{F}_N^H \tag{4.7}$$

where the components of (4.7) represent the following processing steps:

$\mathbf{X}$:	Matrix of input symbols in the delay-Doppler domain
$\mathbf{F}_M \mathbf{X} \mathbf{F}_N^H$:	ISSFT on matrix of delay-Doppler symbols
$\mathbf{F}_M^H$:	Heisenberg transform
$\mathbf{G}_{tx}$:	Pulse shaping
$\mathbf{S}$:	Transmit signal

4.2 OTFS Receiver in Matrix Form

Similar to the transmitter, the OTFS symbols at the receiver in the delay-Doppler domain can be obtained from the OTFS received signal by first performing matched filtering with the respective pulse shape, converting the continuous time receive signal into OTFS symbols in the time-frequency domain using the Wigner transform, and then performing an SFFT to obtain the OTFS symbols in the delay-Doppler domain. Accordingly, the matrix representation of an OTFS receiver can be formulated using (4.3)-(4.6) as

$$\mathbf{Y} = \mathbf{F}_M^H \left(\mathbf{F}_M \mathbf{G}_{rx} \mathbf{R}\right) \mathbf{F}_N = \mathbf{G}_{rx}\mathbf{R}\mathbf{F}_N \tag{4.8}$$

where the components of (4.8) represent the following processing steps:

$\mathbf{R}$:	Matrix of received signals
$\mathbf{G}_{rx}$:	Matched filtering with receiver pulse shape
$\mathbf{F}_M$:	Wigner transform
$\mathbf{F}_M^H (\cdot) \mathbf{F}_N$:	SSFT on matrix of time-frequency received symbols
$\mathbf{Y}$:	Received symbols in the delay-Doppler domain

4.3 OTFS Input-Output Relation Using a Channel Matrix Representation

Let us recall the input-output relationship in the time-frequency domain including additive white Gaussian noise $w(t)$ as

$$r(t) = \int_{-\infty}^{\infty} S(\nu,\tau)s(t-\tau)e^{j2\pi\nu(t-\nu)}d\nu d\tau + w(t) \tag{4.9}$$

The input-output relationship in (4.9) considers a general multipath propagation environment with a continuum of scatterers which includes the special scenario having P discrete specular scatterers (ideal point scatteres). In the delay-Doppler domain, the ith discrete propagation path is associated with a complex attenuation factor h_i, time delay τ_i, and Doppler frequency ν_i. The delay-Doppler channel may then be formulated as

$$S(\tau,\nu) = \sum_{i=1}^{P} h_i\delta(\tau-\tau_i)\delta(\nu-\nu_i) \tag{4.10}$$

Given the discrete delay-Doppler channel in (4.10), the input-output relationship can be expressed in discrete form with l_i and k_i being the discrete delay and Doppler variable, respectively, as [3]

$$r[n] = \sum_{i=1}^{P} h_i e^{j\frac{2\pi k_i(n-l_i)}{MN}} s([n-l_i]_{MN}) + w[n], \quad 0 \le n \le MN-1 \tag{4.11}$$

Similar as the double sums used in the transforms among the different domains can be expressed in matrix form, the input and output symbols $s[n]$ and $r[n]$ can be arranged as vectors $\mathbf{s}$ and $\mathbf{r}$, respectively, allowing to write the input-output relationship as a vector-matrix operation [9]:

$$\mathbf{r} = \mathbf{H}\mathbf{s} + \mathbf{w} \tag{4.12}$$

A discrete delay-Doppler channel matrix $\mathbf{H}$ can be formulated from the set of equations that are obtained from (4.11) for $n = 0, 1, \ldots, MN-1$ giving [9]

$$\mathbf{H} = \sum_{i=1}^{P} h_i \mathbf{\Pi}^{l_i} \mathbf{\Delta}^{k_i} \tag{4.13}$$

Similar to OFDM, the permutation matrix $\mathbf{\Pi}$ in (4.13) causes a forward cyclic shift with respect to the delay and is defined as

$$\mathbf{\Pi} = \begin{Bmatrix} 0 & 0 & \cdots & 0 & 1 \\ 1 & 0 & \cdots & 0 & 0 \\ \vdots & \vdots & \ddots & \vdots & \vdots \\ 0 & 0 & \cdots & 0 & 1 \end{Bmatrix} \tag{4.14}$$

while the diagonal matrix $\mathbf{\Delta}^{k_i}$ captures the Doppler shifts in the respective paths:

$$\mathbf{\Delta}^{k_i} = \begin{Bmatrix} 1 & 0 & \cdots & 0 \\ 0 & e^{j\frac{2\pi k_i(1)}{MN}} & \cdots & 0 \\ \vdots & \vdots & \ddots & \vdots \\ 0 & 0 & \cdots & e^{j\frac{2\pi k_i(MN-1)}{MN}} \end{Bmatrix} \tag{4.15}$$

Then, the received signal in the delay-Doppler domain can be written as

$$\mathbf{y} = \left[(\mathbf{F}_N \otimes \mathbf{G}_{rx})\mathbf{H}(\mathbf{F}_N^H \otimes \mathbf{G}_{tx})\right]\mathbf{x} + (\mathbf{F}_N \otimes \mathbf{G}_{rx})\mathbf{w} \tag{4.16}$$

In view of (4.16), an effective channel matrix for arbitrary transmit pulses and receive pulses (matched filter) can be defined as

$$\begin{aligned} \mathbf{H}_{eff} &= (\mathbf{F}_N \otimes \mathbf{G}_{rx})\mathbf{H}(\mathbf{F}_N^H \otimes \mathbf{G}_{tx}) \\ &= (\mathbf{I}_N \otimes \mathbf{G}_{rx})(\mathbf{F}_N \otimes \mathbf{I}_M)\mathbf{H}(\mathbf{F}_N^H \otimes \mathbf{I}_M)(\mathbf{I}_N \otimes \mathbf{G}_{tx}) \\ &= (\mathbf{I}_N \otimes \mathbf{G}_{rx})\mathbf{H}_{eff}^{rect}(\mathbf{I}_N \otimes \mathbf{G}_{tx}) \end{aligned} \tag{4.17}$$

where $\mathbf{I}_N$ and $\mathbf{I}_M$ are identity matrices of order N and M, respectively, and $\mathbf{H}_{eff}^{rect}$ denotes the effective delay-Doppler channel for rectangular pulses. Using the matrix representation of the effective delay-Doppler channel, the received signal can be written as

$$\mathbf{y} = \mathbf{H}_{eff}\mathbf{x} + \tilde{\mathbf{w}} \tag{4.18}$$

where the additive noise vector is defined as

$$\tilde{\mathbf{w}} = (\mathbf{F}_N \otimes \mathbf{G}_{rx})\mathbf{w} \tag{4.19}$$

CHAPTER 5

Multiple-Input Multiple-Output OTFS

The OTFS input-output relation in matrix form presented in the previous chapter for a single-input single-output (SISO) system can be readily applied to a MIMO-OTFS system [10]. A block diagram of a MIMO-OTFS modulation system is shown in Figure 5.1 with multiple paths from the transmitter to the receiver. In general, the transmit antenna array comprises of N_T antenna elements and the receive antenna array is equipped with N_R. As such, each antenna chain at the transmitter performs a pre-processing and the Heisenberg transform while each antenna chain at the receiver performs the Wigner transform and a post-processing. In the sequel, it is shown that the input-output relation of an MIMO-OTFS system can be discribed in matrix form similar as for a SISO-OTFS system by using an equivalent MIMO channel matrix.

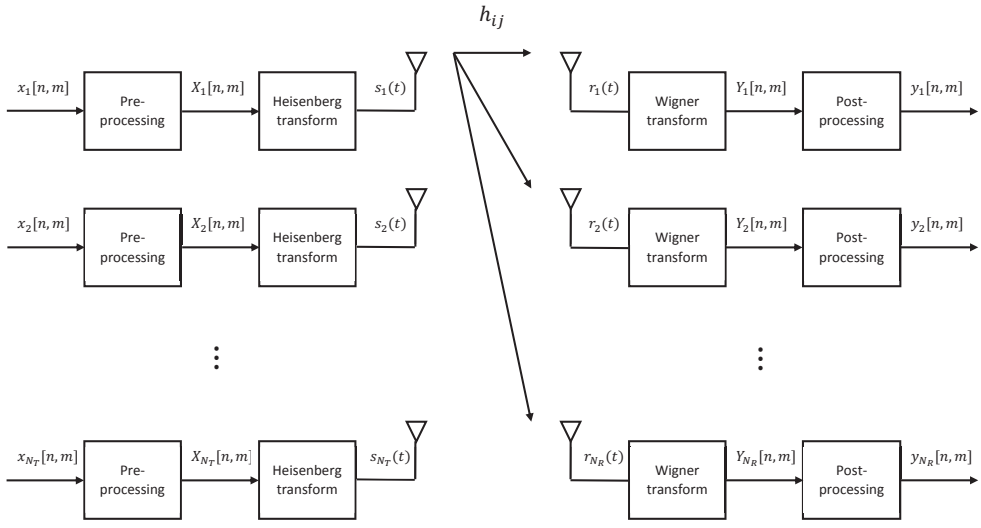

Figure 5.1: Block diagram of a MIMO-OTFS modulation system with N_T transmit antenna elements an N_R receive antenna elements.

Mathematically, the input-output relationship for a MIMO-OTFS system in matrix form can be expressed as [10]

$$\begin{aligned}
\mathbf{y}_1 &= \mathbf{H}_{11}\mathbf{x}_1 + \mathbf{H}_{12}\mathbf{x}_2 + \cdots + \mathbf{H}_{1N_T}\mathbf{x}_{N_T} + \mathbf{n}_1 \\
\mathbf{y}_2 &= \mathbf{H}_{21}\mathbf{x}_1 + \mathbf{H}_{22}\mathbf{x}_2 + \cdots + \mathbf{H}_{2N_T}\mathbf{x}_{N_T} + \mathbf{n}_2 \\
&\vdots \\
\mathbf{y}_{N_R} &= \mathbf{H}_{N_R1}\mathbf{x}_1 + \mathbf{H}_{N_R2}\mathbf{x}_2 + \cdots + \mathbf{H}_{N_RN_T}\mathbf{x}_{N_T} + \mathbf{n}_{N_R}
\end{aligned} \tag{5.1}$$

where $\mathbf{H}_{ij}$ denotes the equivalent channel matrix from the i-th transmit antenna to the j-th receive antenna, and $\mathbf{n}_j$ represents the equivalent noise vector with respect to the j-th receive antenna.

A more compact vectorized formulation of the input-output relation of the MIMO-OTFS system can be given as [10]

$$\mathbf{y}_{MIMO} = \mathbf{H}_{MIMO} \cdot \mathbf{x}_{MIMO} + \mathbf{n}_{MIMO} \tag{5.2}$$

where the equivalent MIMO channel matrix $\mathbf{H}_{MIMO}$ is defined as

$$\mathbf{H}_{MIMO} = \begin{bmatrix} \mathbf{H}_{11} & \mathbf{H}_{12} & \cdots & \mathbf{H}_{1N_T} \\ \mathbf{H}_{21} & \mathbf{H}_{22} & \cdots & \mathbf{H}_{2N_T} \\ \vdots & \vdots & \ddots & \vdots \\ \mathbf{H}_{N_R1} & \mathbf{H}_{N_R2} & \cdots & \mathbf{H}_{N_RN_T} \end{bmatrix} \tag{5.3}$$

and

$$\mathbf{x}_{MIMO} = \left[\mathbf{x}_1^T, \mathbf{x}_2^T, \ldots, \mathbf{x}_{N_T}^T\right]^T \tag{5.4}$$

$$\mathbf{y}_{MIMO} = \left[\mathbf{y}_1^T, \mathbf{y}_2^T, \ldots, \mathbf{y}_{N_R}^T\right]^T \tag{5.5}$$

$$\mathbf{n}_{MIMO} = \left[\mathbf{n}_1^T, \mathbf{n}_2^T, \ldots, \mathbf{n}_{N_R}^T\right]^T \tag{5.6}$$

CHAPTER 6

Simulation Results

In the following sections, we provide simulation results to assess the performance of OFDM modulation in terms of BER for a variety of scenarios:

- Fixed velocity, varied carrier frequency, and 1 path channel
- Varied velocity, fixed carrier frequency, and 1 path channel
- Varied velocity, varied carrier frequency, and 2 paths channel
- MIMI-OTFS aiming to achieve high capacity
- MIMO-OTFS aiming to achieve high reliability

The simulation parameters shown in Table 6.1 have been selected as being representative for the considered directed air data link.

Table 6.1: Simulation Parameters.

Physical Layer		
Carrier frequency	f_c	13 GHz, 18 GHz
Velocity	v	700 km/h, 1235 km/h (speed of sound)
Doppler shift	$f_{D,max}$	8.425 kHz, 11.666 kHz, 14.865 kHz, 20.580 kHz
Bandwidth	B	5 Mbps
Modulation	Type	4-QAM
Channel		
2-ray model	Path 1	Relative delay 0 μs
	Path 2	Relative delay 2 μs
Number of Delay-Doppler Bins Used for OFDM Modulation		
Delay bins	N	32
Doppler bins	M	32
MIMO-OTFS		
Transmit antenna	N_T	2
Receive antenna	N_R	2

The simulation results reported in the subsequent sections, in brief, indeed support the following conjectures:

- OFTS modulation can deal with high Doppler spread.
- Multipath propagation can be exploited to improve BER performance.
- MIMO-OFDM with 2 transmit antenna elements and 2 receive antenna elements can improve both capacity and reliability.
- MIMO-OTFS with 2 transmit antenna elements and 2 receive antenna elements can significantly improved reliability if capacity requirements are relaxed.

6.1 Bit Error Rate of OTFS

First, the impact of the carrier frequency and velocity on the BER of OTFS modulation performance is assessed. Two propagation scenarios are considered: 1 path model (direct link) and 2 paths model (direct link and reflected path).

Figure 6.1 shows the BER performance of the OTFS modulation versus signal-to-noise ratio (SNR) for the 1 path model. The velocity is set to $v = 1235$ km/h while the carrier frequencies are selected as $f_c = 13$ GHz and $f_c = 18$ GHz. These parameters result in the respective maximum Doppler frequencies of $f_{D,max} = 14.865$ kHz and $f_{D,max} = 20.580$ kHz. It can be seen from the figure that OTFS modulation indeed is able to cope with the different Doppler shifts with the observed performance virtually the same for the low to mid-range SNR regime irrespective of the carrier frequency. In the high SNR regime approaching 20 dB, the BER for $f_c = 13$ GHz slightly outperforms that for $f_c = 18$ GHz which may be due to the choice of the number of frequency bins and delay bins. Further studies may be needed to investigate the impact of the number of these bins on the BER for different carrier frequencies.

Figures 6.2-6.3 show the BER performance for the two case that the carrier frequency is fixed to $f_c = 13$ GHz and $f_c = 18$ GHz, respectively, but using different velocities of $v = 700$ km/h and $v = 1235$ km/h for each of the carrier frequencies. The maximum Doppler frequencies for the different cases are obtained as

$$\begin{aligned}
f_c = 13 \text{ GHz}; v = 700 \text{ km/h}: &\quad f_{D,max} = 8.425 \text{ kHz} \\
f_c = 13 \text{ GHz}, v = 1235 \text{ km/h}: &\quad f_{D,max} = 14.865 \text{ kHz} \\
f_c = 18 \text{ GHz}; v = 700 \text{ km/h}: &\quad f_{D,max} = 11.666 \text{ kHz} \\
f_c = 18 \text{ GHz}, v = 1235 \text{ km/h}: &\quad f_{D,max} = 20.580 \text{ kHz}
\end{aligned}$$

The results illustrate that OTFS modulation can cope well with the above wide range of Doppler spread providing very similar performance for all of the four cases. However, the high BER of slightly below 1% at an SNR of 20 dB for all considered scenarios would not support a reliable data link but require additional functionality such as error control coding and MIMO systems to improve the performance.

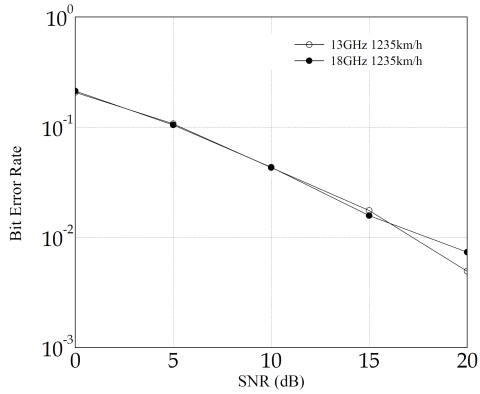

Figure 6.1: BER of OTFS modulation for maximum Doppler spread associated with different carrier frequencies for fixed velocity.

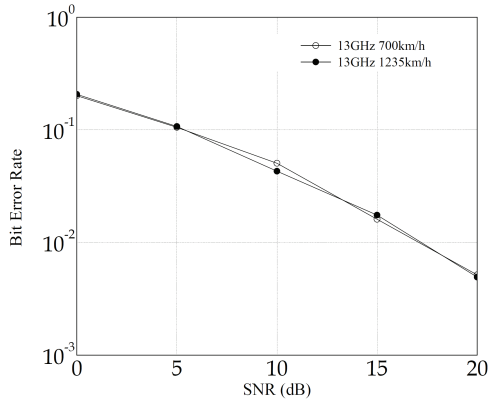

Figure 6.2: BER of OTFS modulation for maximum Doppler spread associated with different velocities and fixed carrier frequency of $f_c = 13$ GHz.

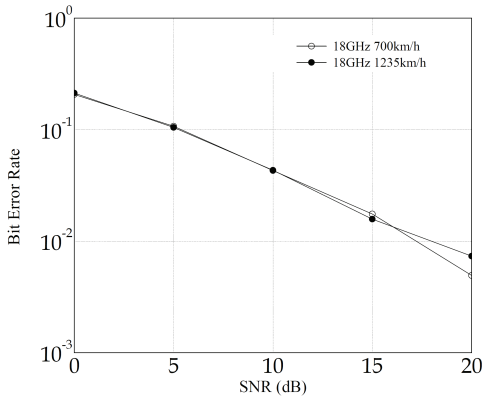

Figure 6.3: BER of OTFS modulation for maximum Doppler spread associated with different velocities and fixed carrier frequency of $f_c = 18$ GHz.

Figure 6.4 compares the BER performance of OTFS modulation obtained for a 1 path channel and a 2 paths channel. The results indicate that exploiting multipath propagation improves the BER performance of OTFS modulation. In the considered scenario, the improvement obtained over the 2 paths channel compared to the 1 path channel increases with the increase of the SNR. For example, at an SNR of 20 dB, the BER of around 1% over the 1 path channel is improved to around 0.1% for the 2 path channel. Further studies on the option of exploring multipath propagation may include the impact of the delay profile of the 2 paths model such as the relative power between the direct path and the reflected path.

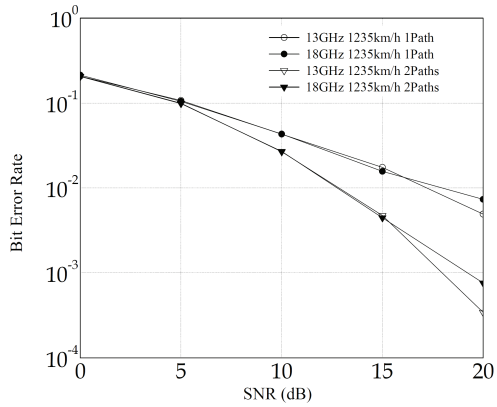

Figure 6.4: BER of OTFS modulation for 1 path and 2 paths channel models.

6.2 Bit Error Rate of MIMO-OTFS

Although multipath propagation can be explored for BER performance improvement, as has been illustrated in the previous section, there are little options to control the propagation environment in the considered application of a directed air data link. As such, a wide range of alternative processing functionalities can be used at the transmitter and receiver providing a large degree of options for system performance improvement. In this section, we combine MIMO systems with OTFS modulation resulting in a MIMO-OTFS system. Regarding the transmit and receive antenna array of a MIMO system, the respective antenna elements may be used to increase capacity, reliability, or find a trade-off between capacity and reliability. In case that high capacity is of main concern, each of the N_T transmit antenna elements carries a different input signals at a given discrete time instant, i.e., $\mathbf{s} = [s_1, s_2, \ldots, s_{N_T}]$ where the input vector $\mathbf{s}$ holds the input signals s_i, $i = 1, 2, \ldots N_T$ (see Figure 6.5). On the other hand, if high link reliability is of major concern, each of the N_T transmit antenna elements carries the same input signals at a given discrete time instant, i.e., $\mathbf{s} = [s_1, s_1, \ldots, s_1]$ (see Figure 6.7).

Figure 6.6 compares the BER performance of conventional OTFS modulation with a 2×2 MIMO-OTFS system aiming at high capacity, i.e., not exploring the entire potential for improving link reliability. The results show that the 2×2 MIMO-OTFS system, although not having high link reliability as main focus, significantly outperforms conventional OTFS modulation in terms of BER for the selected simulation parameters. In particular, at an SNR of 20 dB, conventional OTFS modulation provides a BER of around 10^{-2} while the 2×2 MIMO-OTFS system achieves a largely improved link reliability with a BER of below 10^{-5}.

Figure 6.7 compares the BER performance of conventional OTFS modulation with a 2×2 MIMO-OTFS system aiming at high link reliability by feeding each transmit antenna element with the same input signal at a given discrete time instant. It can be observed that the MIMO-OTFS system aiming for high link reliability not only significantly outperforms conventional OTFS modulation but also the above MIMO-OTFS system that aimed for high capacity. For example, while the MIMO-OTFS system aiming for high capacity required an SNR of 20 dB to obtained a BER of below 10^{-5}, the MIMO-OTFS system aiming for high link reliability requires an SNR of only 10 dB to achieve the same low BER of below 10^{-5}.

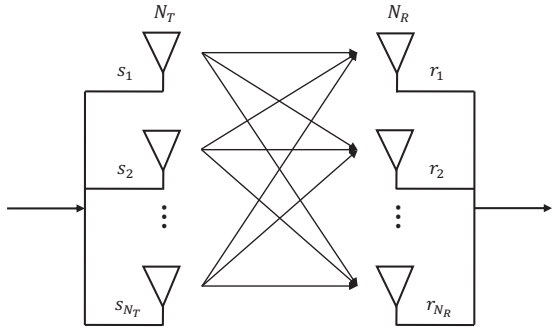

Figure 6.5: MIMO system with N_T transmit antenna elements and N_R receive antenna elements aiming for high capacity by feeding each element with different transmit signals.

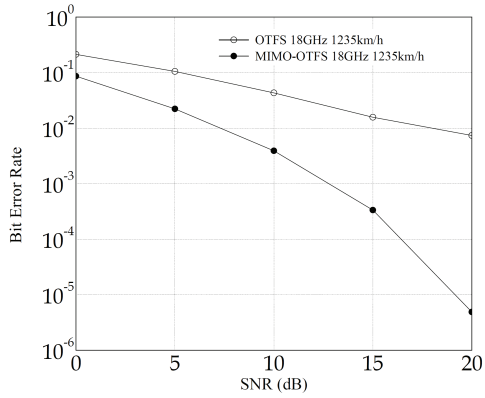

Figure 6.6: BER of the 2×2 MIMO-OTFS system aiming for high capacity.

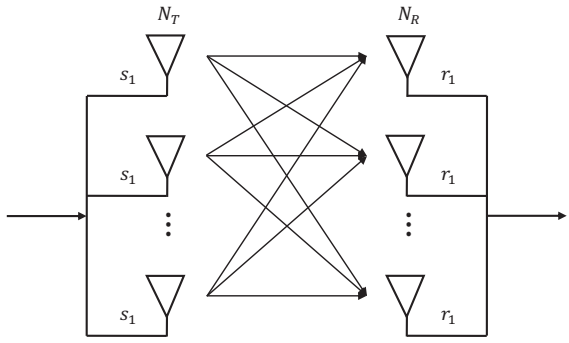

Figure 6.7: MIMO system with N_T transmit antenna elements and N_R receive antenna elements aiming for reliability by feeding each element with the same transmit signal.

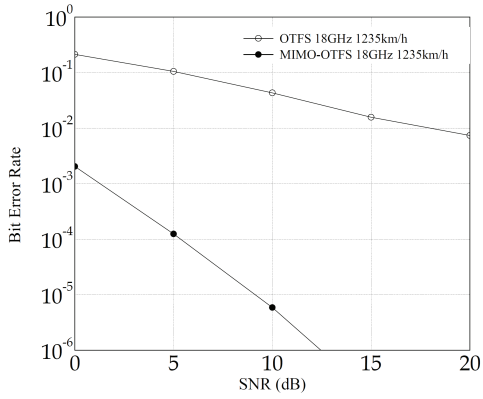

Figure 6.8: BER of the 2×2 MIMO-OTFS system aiming for high link reliability.

CHAPTER 7

Applications

In this chapter, an overview of OTFS applications is provided as follows. Table 7.1 contains surveys on OTFS modulation with focus areas on mobile systems toward 6G, Internet of Things, general aspects of OTFS, and implementation-related topics. Table 7.2 addresses a wide range of general applications of OTFS modulation stretching from OTFS channel estimation to path division multiple access for massive MIMO-OTFS. Table 7.3 is dedicated to OTFS modulation for non-terrestrial networks.

Table 7.1: Surveys on OTFS modulation.

Reference	Survey Focus Areas	Nr. of Refs.
[11]	OTFS as a new delay-Doppler communication paradigm in the context of the evolution of mobile systems toward 6G	139
[12]	Concepts, benefits, and challenges of OTFS for the Internet of Things	148
[13]	State-of-the-art, hotspots, and challenges of OTFS in general	263
[14]	Low complexity detectors for OTFS systems	42
[15]	Concepts, applications, benefits, and challenges of OTFS for non-terrestrial networks.	33

Table 7.2: General applications of OTFS modulation.

References	Applications
[10], [16]–[25]	Detection, channel estimation, parameter estimation
[26]–[33]	Radar applications
[34]–[37]	Integrated sensing and communications
[6], [38]	Software defined radio implementation of OTFS
[39]–[41]	OTFS on static multipath channels
[10], [42]–[47]	MIMO-OTFS and massive MIMO-OTFS
[31], [46], [48]–[51]	OTFS-NOMA
[52]–[55]	Millimeter-wave communication systems
[36], [56]–[64]	V2X communications, high-speed railway
[44]	Path division multiple access for massive MIMO-OTFS
[65]–[67]	Testbeds

Table 7.3: OTFS modulation for non-terrestrial networks.

References	Applications
[68]–[70]	OTFS for unmanned aerial vehicles
[15], [71], [72]	OTFS for airborne communication networks
[43], [73]–[76]	OTFS for satellite networks

Bibliography

[1] R. Hadani, S. Rakib, A. Monk, A. J. Goldsmith, A. F. Molisch, and R. Calderbank, "Orthogonal Time Frequency Space Modulation," in *Proc. IEEE Wireless Communications and Networking Conference*, San Francisco, CA, USA, Mar. 2017, pp. 1–6.

[2] R. Hadani, S. s. Rakib, A. Monk, M. Tsatsanis, and Y. Hebron, "Orthogonal Time Frequency Space Modulation Techniques," U.S. Patent US20200259692A1, Aug. 2020.

[3] Y. Hong, E. Viterbo, and A. Chockalingam, *Orthogonal Time Frequency Space (OTFS) Modulation*, Tutorial at IEEE International Communications Conference, Shanghai, China, May 2019.

[4] P. A. Bello, "Characterization of Randomly Time-Variant Linear Channels," *IEEE Trans. Commun. Systems*, vol. 11, no. 4, pp. 360–393, Apr. 1963.

[5] Z. Wei, W. Yuan, S. Li, J. Yuan, G. Bharatula, R. Hadani, and L. Hanzo, "Orthogonal Time-Frequency Space Modulation: A Promising Next-Generation Waveform," *IEEE Wireless Commun.*, vol. 28, no. 4, pp. 136–144, Aug. 2021.

[6] Z. Wei, S. Li, W. Yuan, R. Schober, and G. Caire, "Orthogonal Time Frequency Space Modulation - Part I: Fundamentals and Challenges Ahead," *IEEE Commun. Letters*, vol. 27, no. 1, pp. 4–8, Jan. 2023.

[7] S. Li, W. Yuan, Z. Wei, R. Schober, and G. Caire, "Orthogonal Time Frequency Space Modulation - Part II: Transceiver Design," *IEEE Commun. Letters*, vol. 27, no. 1, pp. 9–13, Jan. 2023.

[8] W. Yuan, Z. Wei, S. Li, R. Schober, and G. Caire, "Orthogonal Time Frequency Space Modulation - Part III: ISAC and Potential Applications," *IEEE Commun. Letters*, vol. 27, no. 1, pp. 14–18, Jan. 2023.

[9] S. Tiwari, S. S. Das, and V. Rangamgari, "Low-Complexity LMMSE Receiver for OTFS," *IEEE Wireless Commun. Letters*, vol. 23, no. 12, pp. 2205–2209, Dec. 2019.

[10] M. K. Ramachandran and A. Chockalingam, "MIMO-OTFS in High-Doppler Fading Channels: Signal Detection and Channel Estimation," in *Proc. IEEE Global Communications Conference*, Abu Dhabi, United Arab Emirates, Dec. 2018, pp. 1–6.

[11] W. Yuan, S. Li, Z. Wei, J. Jiang, H. Zhang, and P. Fan, "A Survey on Orthogonal Time Frequency Space: New Delay Doppler Communication Paradigm in 6G Era," *China Commun.*, pp. 1–23, Nov. 2022, arXiv:2211.12955v1.

[12] L. Xiao, S. Li, Y. Qian, D. Chen, and T. Jiang, "An Overview of OTFS for Internet of Things: Concepts, Benefits, and Challenges," *IEEE Internet of Things J.*, vol. 9, no. 10, pp. 7596–7618, May 2022.

[13] M. Li, W. Liu, and J. Lei, "A Review on Orthogonal Time-Frequency Space Modulation: State-of-the-Art, Hotspots and Challenges," *Computer Networks*, vol. 224, no. 109597, pp. 1–28, Jan. 2023.

[14] Z. Q. Zhang, H. Liu, Q. L. Wang, and P. Fan, "A Survey on Low Complexity Detectors for OTFS Systems," *ZTE Commun.*, vol. 19, no. 4, pp. 3–15, Dec. 2021.

[15] T. M. C. Chu, H.-J. Zepernick, A. Höök, A. Westerhagen, and B. Granbom, "OTFS Modulation for Non-Terrestrial Networks: Concepts, Applications, Benefits, and Challenges," in *Proc. International Conference on Signal Processing and Communication Systems*, Bydgoszcz, Poland, Sep. 2023.

[16] W. Shen, L. Dai, J. An, P. Fan, and R. W. Heath, "Channel Estimation for Orthogonal Time Frequency Space (OTFS) Massive MIMO," *IEEE Trans. Signal Processing*, vol. 67, no. 16, pp. 4204–4217, Aug. 2019.

[17] X. He, P. Fan, and Q. Wang, "A Two-Stage Channel Estimation Algorithm for OTFS in Fractional Doppler Channels," *IEEE Commun. Letters*, vol. 27, no. 7, pp. 1839–1843, Jul. 2023.

[18] S. P. Muppaneni, S. R. Mattu, and A. Chockalingam, "Channel and Radar Parameter Estimation With Fractional Delay-Doppler Using OTFS," *IEEE Commun. Letters*, vol. 27, no. 5, pp. 1392–1396, May 2023.

[19] H. Shao, H. Zhang, H. Zhou, J. Wang, N. Wang, and A. Nallanathan, "A Complexity-Reduced QRD-SIC Detector for Interleaved OTFS," *IEEE Trans. Wireless Commun.*, vol. 22, no. 2, pp. 950–960, Feb. 2023.

[20] Y. Zhang, Q. Zhang, C. He, and C. Long, "Channel Estimation for OTFS System Over Doubly Spread Sparse Acoustic Channels," *China Commun.*, vol. 20, no. 1, pp. 50–65, Jan. 2023.

[21] Y. Gong, Q. Li, F. Meng, X. Li, and Z. Xu, "Data-Driven Deep Learning for OTFS Detection," *China Commun.*, vol. 20, no. 1, pp. 88–101, Jan. 2023.

[22] X. Wei, L. Li, and Y. Jin, "Channel Estimation Based on Compressed Sensing and Iterative Detection for Zero-Padded OTFS," in *Proc. Information Communication Technologies Conference*, Nanjing, China, Jun. 2023, pp. 34–39.

[23] B. Jia, P. Fan, and Q. Wang, "Low Complexity Doubly Fractional OTFS Channel Estimation Based on L-BFGS Method," in *Proc. IEEE Wireless Communications and Networking Conference*, Glasgow, United Kingdom, May 2023, pp. 1–6.

[24] B. He et al., "Denoising CNN Based Channel Estimation for Vehicular OTFS Communication System," in *Proc. International Conference on Advanced Communication Technology*, Pyeongchang, Republic of Korea, Feb. 2023, pp. 54–58.

[25] Z. Tang, Z. Jiang, W. Pan, and L. Zeng, "The Estimation Method of Sensing Parameters Based on OTFS," *IEEE Access*, vol. 11, pp. 66 035–66 049, Jun. 2023.

[26] A. Correas-Serrano, N. Petrov, M. Gonzalez-Huici, and A. Yarovoy, "Comparison of Radar Receivers for OFDM and OTFS Waveforms," in *Proc. European Radar Conference*, Milan, Italy, Sep. 2022, pp. 1–4.

[27] L. Gaudio, M. Kobayashi, B. Bissinger, and G. Caire, "Performance Analysis of Joint Radar and Communication using OFDM and OTFS," in *Proc. IEEE International Conference on Communications Workshops*, Shanghai, China, May 2019, pp. 1–6.

[28] H. Zhang, T. Zhang, and Y. Shen, "Modulation Symbol Cancellation for OTFS-Based Joint Radar and Communication," in *Proc. IEEE International Conference on Communications Workshops*, Montreal, QC, Canada, Jun. 2021, pp. 1–6.

[29] K. Wu, J. A. Zhang, X. Huang, and Y. J. Guo, "Integrating Low-Complexity and Flexible Sensing Into Communication Systems," *J. Sel. Areas Commun.*, vol. 40, no. 6, pp. 1873–1889, Jun. 2022.

[30] P. Raviteja, K. T. Phan, Y. Hong, and E. Viterbo, "Orthogonal Time Frequency Space (OTFS) Modulation Based Radar System," in *Proc. IEEE Radar Conference*, Boston, MA, USA, Apr. 2019, pp. 1–6.

[31] B. C. Pandey, S. K. Mohammed, P. Raviteja, Y. Hong, and E. Viterbo, "Low Complexity Precoding and Detection in Multi-User Massive MIMO OTFS Downlink," *IEEE Trans. Vehicular Technol.*, vol. 70, no. 5, pp. 4389–4405, May 2021.

[32] S. K. Mohammed, R. Hadani, A. Chockalingam, and R. Calderbank, "OTFS—A Mathematical Foundation for Communication and Radar Sensing in the Delay-Doppler Domain," *IEEE BITS the Inf. Theory Mag.*, vol. 2, no. 2, pp. 36–55, Nov. 2022.

[33] G. Sharma and A. A. B. Raj, "OTFS Based SAR With Low Complexity Receiver," *IEEE Access*, vol. 11, pp. 66 194–66 200, Jun. 2023.

[34] Z. Wei, H. Qu, Y. Wang, X. Yuan, H. Wu, Y. Du, K. Han, N. Zhang, and Z. Feng, "Integrated Sensing and Communication Signals Toward 5G-A and 6G: A Survey," *IEEE Internet of Things J.*, vol. 10, no. 13, pp. 11 068–11 092, Jul. 2023.

[35] K. Wu, J. A. Zhang, X. Huang, and Y. J. Guo, "OTFS-Based Joint Communication and Sensing for Future Industrial IoT," *IEEE Internet of Things J.*, vol. 10, no. 3, pp. 1973–1989, Feb. 2023.

[36] W. Yuan, Z. Wei, J. Y. S. Li, and D. W. K. Ng, "Integrated Sensing and Communication-Assisted Orthogonal Time Frequency Space Transmission for Vehicular Networks," *IEEE J. Sel. Topics in Signal Processing*, vol. 15, no. 6, pp. 1515–1528, Nov. 2021.

[37] O. Zacharia and M. V. Devi, "Fractional Delay and Doppler Estimation for OTFS Based ISAC Systems," in *Proc. IEEE Wireless Communications and Networking Conference*, Glasgow, United Kingdom, Mar. 2023, pp. 1–6.

[38] T. Thaj and E. Viterbo, "OTFS Modem SDR Implementation and Experimental Study of Receiver Impairment Effects," in *Proc. IEEE International Conference on Communications Workshops*, Shanghai, China, May 2019, pp. 1–6.

[39] P. Raviteja, E. Viterbo, and Y. Hong, "OTFS Performance on Static Multipath Channels," *IEEE Wireless Commun. Letters*, vol. 8, no. 3, pp. 745–748, Jun. 2019.

[40] S.-Y. Tsai, W.-C. Chen, and C.-D. Chung, "Iterative Symbol Decision Schemes for CP-OTFS on Static Multipath Channels," in *Proc. International Conference on Computing, Networking and Communications*, Honolulu, HI, USA, Mar. 2023, pp. 704–709.

[41] Z. Wang, X. Chen, and X. Ning, "BER Analysis of Integrated WFRFT-OTFS Waveform Framework Over Static Multipath Channels," *IEEE Commun. Letters*, vol. 25, no. 3, pp. 754–758, Mar. 2021.

[42] Y. Liu, F. Gao, J. Ma, and X. Wang, "Uplink-Aided High Mobility Downlink Channel Estimation Over Massive MIMO-OTFS System," *IEEE J. Sel. Areas Commun.*, vol. 38, no. 9, pp. 1994–2009, Sep. 2019.

[43] B. Shen, Y. Wu, J. An, C. Xing, L. Zhao, and W. Zhang, "Random Access With Massive MIMO-OTFS in LEO Satellite Communications," *IEEE J. Sel. Areas Commun.*, vol. 40, no. 10, pp. 2865–2882, Oct. 2022.

[44] M. Li, F. Gao, P. Fan, and O. A. Dobre, "A New Path Division Multiple Access for the Massive MIMO-OTFS Networks," *IEEE J. Sel. Areas Commun.*, 2020 (Early Access).

[45] A. R. Reyhani, A. Farhang, M. Ji, R. R. Chen, and B. Farhang-Boroujeny, "Analysis of Discrete-Time MIMO OFDM-Based Orthogonal Time Frequency Space Modulation," in *Proc. IEEE International Conference on Communications*, Kansas City, MO, USA, May 2018, pp. 1–6.

[46] W. Shao, S. Zhang, C. Zhong, X. Lei, and P. Fan, "Angle-Delay-Doppler Domain NOMA over Massive MIMO-OTFS Networks," in *Proc. IEEE/CIC International Conference on Communications in China*, Chongqing, China, Aug. 2020, pp. 74–79.

[47] M. J. Bocus, A. Doufexi, and D. Agrafiotis, "Performance of OFDM-Based Massive MIMO OTFS Systems for Underwater Acoustic Communication," *IET Commun.*, vol. 14, no. 4, pp. 588–593, Jan. 2019.

[48] Z. Ding, "Robust Beamforming Design for OTFS-NOMA," *IEEE Open J. of the Commun. Society*, vol. 1, pp. 33–40, Nov. 2020.

[49] A. Chatterjee, V. Rangamgari, S. Tiwari, and S. S. Das, "Nonorthogonal Multiple Access With Orthogonal Time–Frequency Space Signal Transmission," *IEEE Systems J.*, vol. 1, no. 15, pp. 383–394, Mar. 2021.

[50] G. D. Surabhi and A. Chockalingam, "Low-Complexity Linear Equalization for 2×2 MIMO-OTFS Signals," in *Proc. IEEE International Workshop on Signal Processing Advances in Wireless Communications*, Atlanta, GA, USA, May 2020, pp. 1–5.

[51] Z. Ding, R. Schober, P. Fan, and H. V. Poor, "OTFS-NOMA: An Efficient Approach for Exploiting Heterogenous User Mobility Profiles," *IEEE Trans. Commun.*, vol. 67, no. 11, pp. 7950–7965, Nov. 2019.

[52] R. Hadani, S. Rakib, A. F. Molisch, C. Ibars, A. Monk, M. Tsatsanis, J. Delfeld, A. Goldsmith, and R. Calderbank, "Orthogonal Time Frequency Space (OTFS) Modulation for Millimeter-Wave Communications Systems," in *Proc. IEEE MTT-S International Microwave Symposium*, Honololu, HI, USA, Jun. 2017, pp. 681–683.

[53] X. Wu, S. Ma, and X. Yang, "Tensor-Based Low-Complexity Channel Estimation for mmWave Massive MIMO-OTFS Systems," *J. Commun. and Information Networks*, vol. 5, no. 3, pp. 324–334, Sep. 2020.

[54] S. Srivastava, R. K. Singh, A. K. Jagannatham, A. Chockalingam, and L. Hanzo, "OTFS Transceiver Design and Sparse Doubly-Selective CSI Estimation in Analog and Hybrid Beamforming Aided mmWave MIMO Systems," *IEEE Trans. Wireless Commun.*, vol. 21, no. 12, pp. 10 902–10 917, Dec. 2022.

[55] X. Qi and J. Xie, "Cubature Kalman Filter Based Millimeter Wave Beam Tracking for OTFS Systems," *China Commun.*, vol. 20, no. 7, pp. 233–240, Jul. 2023.

[56] A. Pfadler, P. Jung, and S. Stanczak, "Pulse-Shaped OTFS for V2X Short-Frame Communication with Tuned One-Tap Equalization," in *Proc. International ITG Workshop on Smart Antennas*, Hamburg, Germany, Feb. 2020, pp. 1–6.

[57] W. Anwar, A. Krause, A. Kumar, N. Franchi, and G. P. Fettweis, "Performance Analysis of Various Waveforms and Coding Schemes in V2X Communication Scenarios," in *Proc. IEEE Wireless Communications and Networking Conference*, Seoul, Republic of Korea, May 2020, pp. 1–8.

[58] H. Groll et al., "Sparsity in the Delay-Doppler Domain for Measured 60 GHz Vehicle-to-Infrastructure Communication Channels," in *Proc. IEEE International Conference on Communications Workshops*, Shanghai, China, May 2019, pp. 1–6.

[59] Y. Ma, G. Ma, N. Wang, Z. Zhong, and B. Ai, "OTFS-TSMA for Massive Internet of Things in High-Speed Railway," *IEEE Trans. Wireless Commun.*, vol. 21, no. 1, pp. 519–531, Jan. 2022.

[60] T. Blazek and D. Radovic, "Performance Evaluation of OTFS Over Measured V2V Channels at 60 GHz," in *Proc. IEEE MTT-S International Conference on Microwaves for Intelligent Mobility*, Linz, Austria, Nov. 2020, pp. 1–4.

[61] D. Radovic, C. F. Mecklenbräuker, and T. Blazek, "OTFS Performance Over Different Measured Vehicular 60 GHz Millimeter-Wave Channels," in *Proc. International Conference on Software, Telecommunications and Computer Networks*, Split, Hvar, Croatia, Sep. 2021, pp. 1–5.

[62] H. Shang et al., "OTFS Modulation and PAPR Reduction for IoT-Railways," *China Commun.*, vol. 20, no. 1, pp. 102–113, Jan. 2023.

[63] S. K. Dehkordi, J. C. Hauffen, P. Jung, R. Hernangomez, G. Caire, and S. Stanczak, "Multi-Scatter-Point Target Estimation for Sensing-Assisted OTFS Automotive Communication," in *Proc. International ITG Workshop on Smart Antennas and Conference on Systems, Communications, and Coding*, Braunschweig, Germany, Feb. 2023, pp. 1–6.

[64] W. Yuan, J. Zou, Y. Cui, X. Li, J. Mu, and K. Han, "Orthogonal Time Frequency Space and Predictive Beamforming-Enabled URLLC in Vehicular Networks," *IEEE Wireless Commun.*, vol. 30, no. 2, pp. 56–62, Apr. 2023.

[65] R. Marsalek, J. Blumenstein, D. Schützenhöfer, and M. Pospisil, "OTFS Modulation and Influence of Wideband RF Impairments Measured on a 60 GHz Testbed," in *Proc. IEEE International Workshop on Signal Processing Advances in Wireless Communications*, Atlanta, GA, USA, May 2020, pp. 1–5.

[66] P. Karpovich, T. P. Zielinski, R. Maksymiuk, K. Abratkiewicz, P. Tomikowski, and P. Samczyński, "Experimental Testing of an OTFS-Modulated Waveform in a Joint Radar-Comm System," in *Proc. IEEE Radar Conference*, San Antonio, TX, USA, May 2023, pp. 1–6.

[67] N. Tawa, T. Kuwabara, Y. Maruta, and T. Kaneko, "28 GHz Over-the-Air Measurement Using an OTFS Multi-User Distributed MIMO," in *Proc. European Microwave Conference*, London, United Kingdom, Jun. 2022, pp. 450–453.

[68] F. Linsalata, A. Albanese, V. Sciancalepore, F. Roveda, M. Magarini, and X. Costa-Perez, "OTFS-Superimposed PRACH-Aided Localization for UAV Safety Applications," in *Proc. IEEE Global Communications Conference*, Madrid, Spain, Dec. 2021, pp. 1–6.

[69] R. Han, J. Ma, and L. Bai, "Tractory Planning for OTFS-Based UAV Communications," *China Commun.*, vol. 20, no. 1, pp. 114–124, Jan. 2023.

[70] S. K. Mohammed, "Time-Domain to Delay-Doppler Domain Conversion of OTFS Signals in Very High Mobility Scenarios," *IEEE Trans. Vehicular Technol.*, vol. 70, no. 6, pp. 6178–6183, Jun. 2021.

[71] T. M. C. Chu, H.-J. Zepernick, A. Westerhagen, A. Höök, and B. Granbom, "Performance Assessment of OTFS Modulation in High Doppler Airborne Communication Networks," *Mobile Networks and Applications*, vol. 27, pp. 1746–1756, Aug. 2022.

[72] ——, "Performance of OTFS Modulation Over Rician Channels in Airborne Communication Networks," in *Proc. International Telecommunication Networks and Applications Conference*, Wellington, New Zealand, Nov. 2022, pp. 1–6.

[73] J. Shi, J. Hu, Z. Tie, W. Liang, and Z. Ding, "OTFS Enabled LEO Satellite Communications: A Promising Solution to Severe Doppler Effects," *IEEE Network*, pp. 1–7, 2023 (Early Access).

[74] M. Yiyan, M. Guoyu, Z. Zhangdui, and A. Bo, "OTFS Enabled NOMA for mMTC Systems Over LEO Satellite," *ZTE Commun.*, vol. 19, no. 4, pp. 63–70, Dec. 2021.

[75] J. Shi, J. Hu, Y. Yue, X. Xue, W. Liang, and Z. Li, "Outage Probability for OTFS Based Downlink LEO Satellite Communication," *IEEE Trans. Vehicular Technol.*, vol. 71, no. 3, pp. 3355–3360, Mar. 2022.

[76] X. Zhou, K. Ying, Z. Gao, Y. Wi, Z. Xiao, S. Chatzinotas, J. Yuan, and B. Ottersten, "Active Terminal Indentification, Channel Estimation, and Signal Detection for Grant-Free NOMA-OTFS in LEO Satellite Internet-of-Things," *IEEE Trans. Wireless Commun.*, vol. 22, no. 4, pp. 2847–2866, Apr. 2023.